

Research paper

Analysis of Bottom Reverberation Intensity Under Beam-Controlled Emission Conditions in Deep Water

Guangying ZHENG^{(1),(2),(3)*}, Xiaowei GUO^{(1),(2),(3)**}, Fangwei ZHU^{(1),(2),(3)},
Fangyong WANG^{(1),(2),(3)}, Linlang BAI^{(1),(2),(3)}

⁽¹⁾ *Science and Technology on Sonar Laboratory*
Hangzhou, China

⁽²⁾ *Hangzhou Applied Acoustics Research Institute*
Hangzhou, China

⁽³⁾ *Hanjiang National Laboratory*
Wuhan, China

Corresponding Authors' e-mails: *276454158@qq.com, **645494944@qq.com

(received October 29, 2023; accepted December 13, 2023; published online March 4, 2024)

A comprehensive understanding of the characteristics and the formation mechanism of reverberation is the key to improving the performance of the active target detection. In response to the challenge of analyzing the intensity of bottom reverberation in typical deep-sea environments, this study proposes a prediction method for the bottom reverberation intensity under beam-controlled emission conditions. It explains the variation law of bottom reverberation intensity under beam-controlled emission conditions in typical deep-sea environments of the South China Sea through theoretical and simulation analyses. Reverberation intensity of the deep-sea bottom under beam-controlled emission conditions exhibits significant fluctuations during the duration of reverberations in the direct sound zone of the seabed. This phenomenon is closely related to the directionality of the source emission, leading to intermittent reverberation masking and detectable areas in the active sonar detection. In addition, the duration of the high-reverberation zone near the cutoff distance of the direct sound from the seabed is longer under the beam-controlled emission conditions of the emission array located within the surface waveguide layer of the deep sea during winter.

Keywords: bottom reverberation; deep water; beam controlled emission; ray theory.



Copyright © 2024 The Author(s).
This work is licensed under the Creative Commons Attribution 4.0 International CC BY 4.0
(<https://creativecommons.org/licenses/by/4.0/>).

1. Introduction

Reverberation is the primary background interference in the active sonar target detection, and a comprehensive understanding of its characteristics and formation mechanism is the key to improving the performance of the active target detection (CUI *et al.*, 2023; HAO *et al.*, 2023). Meanwhile, reverberation carries hidden ocean information that can be used for environmental parameter inversion, leading to the increasing attention toward reverberation research in the field of marine acoustics. At present, theoretical and experimental studies on shallow water reverberation are relatively more common than those on deep water.

With regard to the reverberation prediction theory, domestic and foreign scholars have established the theory of normal mode reverberation (ZHANG *et al.*, 1987), the theory of ray reverberation (LUPIEN *et al.*, 1995), and the theory of parabolic equation reverberation (COLLINS, EVANS, 1992). The intensity attenuation characteristics and spatial correlation characteristics of reverberation signals combined with experimental research have been simultaneously analyzed. Hence, the current study no longer develops this topic.

The characteristics of deep sea reverberation are significantly different from those of shallow sea reverberation, and their analysis and numerical modeling methods are different. A large number of the-

oretical and experimental studies on deep-sea reverberation have been conducted in the last century. [ELLIS](#) and [CROWE](#) (1991) proposed a 3D seabed scattering function that included backscattering and lateral scattering based on the Lambert scattering model. This function was used in the numerical simulation of deep-sea bistatic reverberation and compared with experimental results. [MACKENZIE](#) (1961) calculated the deep-sea bottom reverberation of near-bottom sound sources and receivers at specific frequencies and explained the applicable angle range of the scattering formula. [URICK](#) and [SALING](#) (1962) calculated the seabed backscatter excited by an explosive sound source and obtained a scattering intensity curve with angle. [ELLIS](#), [HALLER](#) (1987), and [ELLIS](#), [CROWE](#) (1991) combined the Lambert scattering model with the surface scattering function based on the Kirchhoff approximation to propose a 3D seabed scattering function that included backscattering and lateral scattering. They used it in the numerical simulation of deep-sea bistatic reverberation and compared it with experimental measurement results. [WILLIAMS](#) and [JACKSON](#) (1998) used the Kirchhoff approximation and the perturbation theory to describe the seafloor backscattering while discussing the effects of seafloor sediment layers and substrates on scattering.

With the support of relevant national plans, significant improvements have been achieved in recent years in experimental methods and equipment for deep-sea acoustics in China. A large number of deep-sea experiments have been conducted, promoting theoretical and experimental research on deep-sea bottom reverberation. [WENG et al.](#) (2014) conducted numerical simulations of local deep-sea bottom reverberation by using the ray method and provided preliminary explanations and analyses of experimental data. [GUO et al.](#) (2009) proposed an incoherent bottom reverberation signal model based on ray theory; this model simplified the calculation of the reverberation signal prediction. [XU et al.](#) (2016) calculated deep-sea reverberation generated by the first bottom reflection of sound waves and obtained numerical results that were consistent with experimental data. [QIN et al.](#) (2019) proposed a deep-sea bottom reverberation model based on the ray theory for calculating local and bistatic reverberation and then compared the experimental data with the simulation results to obtain the seabed scattering coefficient of the experimental sea area. [XUE et al.](#) (2021) described interface reverberation as an incoherent superposition of different multipath reverberation fading processes and combined it with the physical mechanism of interface scattering. They established a reverberation intensity model with the physical parameters of the sea surface and seabed as variables.

The current study focuses on deep sea bottom reverberation characteristics under beam-controlled emission conditions in the actual work of active sonar.

It introduces a prediction method for deep sea bottom reverberation under beam-controlled emission conditions and explains the formation mechanism of deep sea bottom reverberation fluctuation laws through theoretical and simulation analyses.

2. Methodology

2.1. Model of deep-sea bottom reverberation intensity under beam-controlled emission conditions

The description of sound propagation in accordance with the ray theory is simple and intuitive, and thus, it is extremely helpful for explaining the results of other sound propagation models. Simultaneously, it directly establishes the relationship between the sound propagation distance and propagation time; hence, it can be used to predict reverberation intensity in high-frequency situations in the deep sea. Accordingly, this study uses the ray theory to establish a deep-sea bottom reverberation model for simulation analysis.

Reverberation signals can be expressed as the process of propagating sound signals excited by a sound source to a seafloor scatterer and then scattering them back to the receiver. Figure 1 shows a diagram of the formation of deep-sea bottom reverberation in the case of a combined transmitter and receiver. Considering that beam control in practical active sonar applications is generally the pitch angle, i.e., the vertical beam control, this study abstracts it as a vertical dimension emission array to study deep-sea bottom reverberation intensity characteristics under beam-controlled emission conditions.

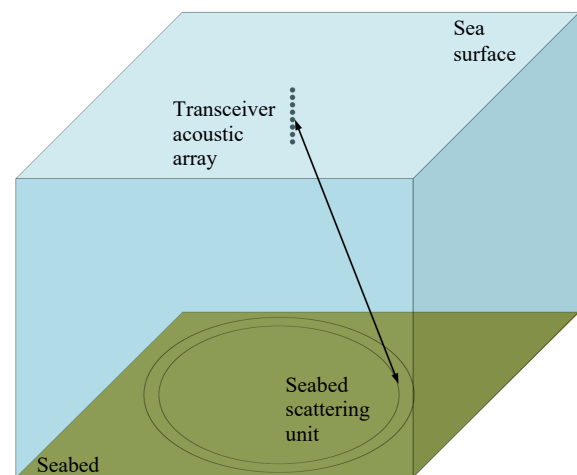


Fig. 1. Schematic of seabed scatterer division under beam-controlled emission conditions.

In the case of directional emission from a transceiver acoustic array, p_{inc} denotes the sound pressure transfer function from the sound source to the seabed scattering element under directional sound source radiation, p_{scatt} represents the sound pressure transfer

function from the seabed scattering element to the transceiver array under omnidirectional sound source radiation, \mathbf{r}_i denotes the i -th eigenray, and the intensity of the incident wave propagating along the incident eigenray to the seabed scattering element ds is represented as $p_{\text{inc}}^2(\mathbf{r}_i)$. The scattering wave intensity scattered by the seabed scattering unit ds can be expressed as

$$p_{\text{inc}}^2(\mathbf{r}_i) f(\theta_{\text{inc}}, \theta_{\text{scatt}}) ds, \quad (1)$$

where $f(\theta_{\text{inc}}, \theta_{\text{scatt}})$ represents the backscatter function of the seabed, which is affected by the incident and scattering grazing angles, and ds is the area of the scattering unit. The reverberation intensity incident along the i -th eigenray to the scattering element returning to the receiving point along the j -th eigenray can be expressed as (XUE *et al.*, 2021):

$$I_{\text{scatt}(ij)} = \int p_{\text{inc}}^2(\mathbf{r}_i) f(\theta_{\text{inc}}, \theta_{\text{scatt}}) p_{\text{scatt}}^2(\mathbf{r}_j) ds. \quad (2)$$

The total bottom reverberation intensity at the receiving array is the sum of the reverberations that arrive along all the propagation paths (XUE *et al.*, 2021):

$$I_{\text{scatt}} = \sum_{i=1}^N \sum_{j=1}^M \int p_{\text{inc}}^2(\mathbf{r}_i) f(\theta_{\text{inc}}, \theta_{\text{scatt}}) p_{\text{scatt}}^2(\mathbf{r}_j) ds, \quad (3)$$

where N represents the number of incident eigenrays, and M represents the number of scattered eigenrays that correspond to the i -th incident eigenray, I_{scatt} is the total reverberation intensity.

The prerequisite for predicting the intensity of deep-sea bottom reverberation under beam-controlled emission conditions is the prediction of the deep-sea sound field transfer function under beam-controlled conditions and seabed scattering characteristics. The current study utilizes the ray model sound field calculation program BELHOP to predict the eigenray and the corresponding grazing angle, time delay, and the transfer function under directional source conditions. Meanwhile, a small-slope approximation (SSA) model is used to predict the seabed scattering characteristic.

2.2. SSA model

In this study, the small slope formalism is adopted for bottom interface scattering. This lowest-order SSA (THORSOS, BROCHAT, 1995; BROCHAT, THORSOS, 1997) models interface scattering strength in all orders of the surface height h and through the first-order derivatives of h (surface slope). Using the local SSA instead of the standard first-order perturbation approximation improves prediction accuracy at the cost of moderately increasing numerical complexity.

The SSA result for an incoherent component of the scattering cross section per unit area (per unit

solid angle) for a random, rough interface is as follows (GRAUSS *et al.*, 2002):

$$\sigma \frac{1}{8} \left| \frac{\beta}{|Q_h| Q_z} \right|_{\text{int}}^2, \quad (4)$$

where β is an algebraic form that depends on the boundary conditions that are prevailing at the interface. $|Q_h|$ and Q_z are given by (GRAUSS *et al.*, 2002):

$$|Q_h| = k_0 \sqrt{a^*}, \quad (5)$$

$$Q_z = -k_0 (\sin \theta_{\text{inc}} + \sin \theta_{\text{scatt}}), \quad (6)$$

where $a^* = \cos^2 \theta_{\text{inc}} + \cos^2 \theta_{\text{scatt}} - 2 \cos \theta_{\text{inc}} \cos \theta_{\text{scatt}} \cos \phi_{bi}$ and $k_0 = \frac{2\pi f}{c_0}$ denotes the acoustic wavenumbers; θ_{inc} denotes the incident grazing angle; θ_{scatt} denotes the scattered grazing angle; ϕ_{bi} denotes the bistatic angle, which is defined as the difference in azimuth between the incident and scattered directions; I in Eq. (7) denotes the integral that involves the spatial spectrum of roughness, and it is given by (GRAUSS *et al.*, 2002):

$$I(\alpha) = \int_0^\infty J_0(y) y \exp(-\alpha y^{2\nu}) dy, \quad (7)$$

where $\nu \equiv \frac{(\gamma_2 - 2)}{2}$, γ_2 denotes the roughness spectral exponent, with $\gamma_2 \in (2, 4)$, J_0 is the 0-th-order Bessel function of the first kind, and α is given by (GRAUSS *et al.*, 2002):

$$\alpha = \frac{(h_{\text{rms}} Q_z)^2 \Gamma(1 - \nu)}{(2h_0 |Q_h|)^{2\nu} \Gamma(1 + \nu)}, \quad (8)$$

where h_{rms}^2 denotes the mean-square roughness, which is given by (GRAUSS *et al.*, 2002):

$$h_{\text{rms}}^2 = \frac{\pi w_2}{h_0^2 \nu}, \quad (9)$$

where w_2 is the input rough spectral intensity, and h_0 is a normalizing reference distance of 1 m.

Notably, once the real or imaginary part of a sound speed acquires dependence on frequency, then α , β , and σ_{int} acquire complicated frequency dependencies.

3. Analysis of deep-sea sound field characteristics under beam-controlled conditions

This section conducts a simulation analysis of the sound field distribution under the conditions of omnidirectional and directional sound sources as a prerequisite for the simulation analysis of deep-sea bottom reverberation under beam-controlled emission conditions.

The simulation analysis focuses on the typical deep-sea hydrological environment of the South China Sea,

with a depth of 4000 m. The historically measured summer and winter sound speed profiles are presented in Fig. 2. The material of the seabed is fine sand, with a sound speed of 1753 m/s, a density of 1.957 g/cm^3 , and an attenuation coefficient of $0.51 \text{ dB/m} \cdot \text{Hz}$. To compare the changes in the sound field distribution caused by beam-controlled emission, simulation calculations were conducted using the BELLHOP (PORTER, 2011) ray model sound field calculation program, and sound field distributions were given for omnidirectional and directional source emission cases. The sound source array under beam-controlled emission conditions is an eight-element vertical array, with a center frequency of 1 kHz. The array elements are arranged at a half-wavelength spacing of 0.75 m, and the center depth of the array is arranged at a depth of 10 m underwater, such that the depth of the entire sound source array is within 50 m. The array is arranged inside the surface waveguide to illustrate sound field differences during winter when a surface waveguide is present. The natural directionality of the eight-element transceiver combined with a vertical array is shown in Fig. 3. Its main lobe corresponds to 0° , with the first side lobe appear-

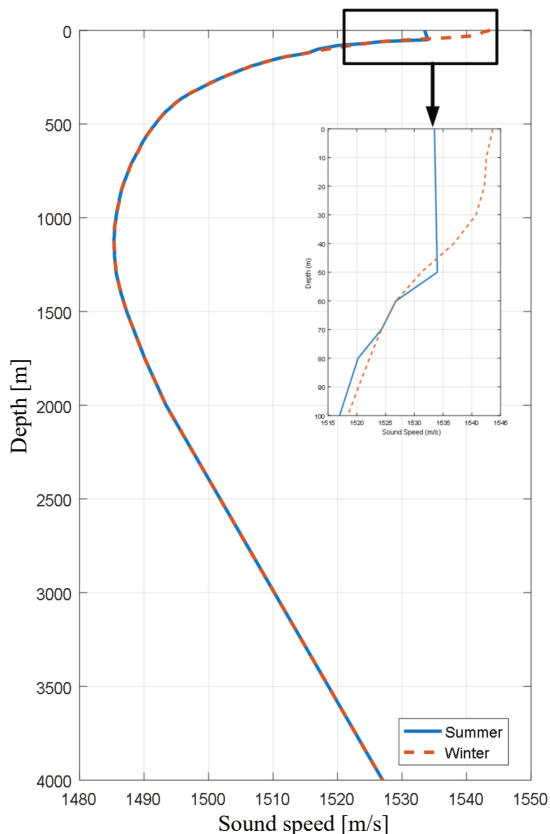


Fig. 2. Sound speed profile (SSP) in deep water. The blue solid line represents the summer sound speed profile, while the red dashed line represents the winter sound speed profile. The subplot of Fig. 2 gives the variation of the SSP over a depth range of 100 m, emphasizing the difference between the summer and winter SSP, i.e., a surface isothermal layer of 50 m occurs during winter in blue solid line.

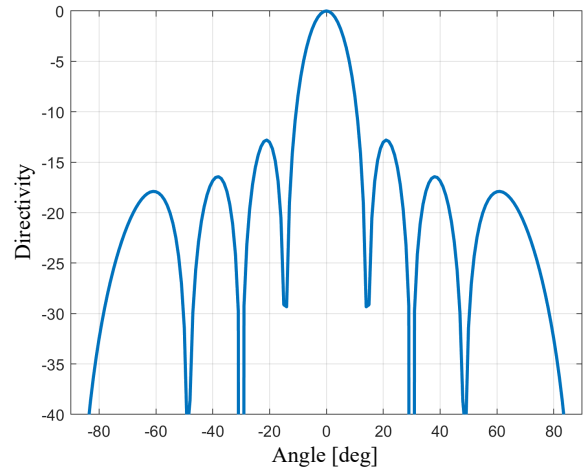
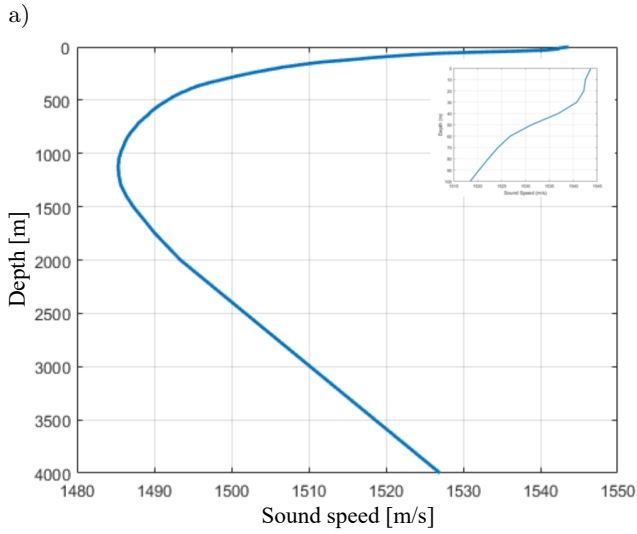


Fig. 3. Natural directivity of eight-element source array.

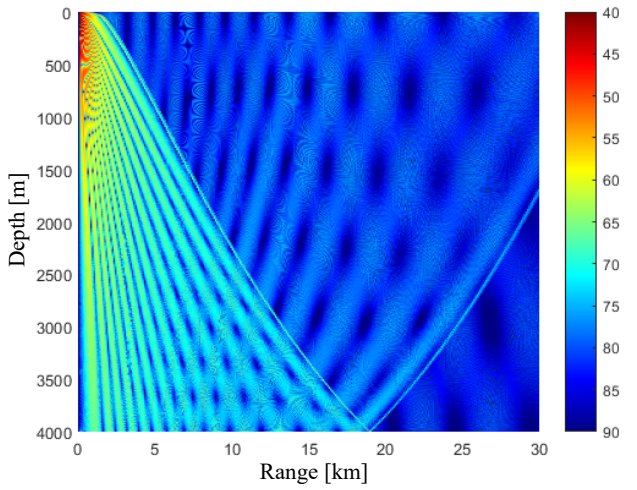
ing at an angle of $\pm 21^\circ$, the second side lobe appearing at an angle of $\pm 38^\circ$, and the third side lobe appearing at an angle of $\pm 61^\circ$.

The distribution of sound fields excited by directional and omnidirectional sources in the deep sea of the South China Sea during summer is shown in Fig. 4. In contrast with the excited sound field of omnidirectional sources, the main energy emitted by directional sources leads to a clear high-sound-intensity region at 18–19 km, which corresponds to the main lobe with a grazing angle of 0° in the directional pattern. The leakage of the side-lobe energy leads to intermittent high-sound-intensity regions within the range of 0–15 km. The high-sound-intensity region at 10 km corresponds to the first side lobe with a grazing angle of $\pm 21^\circ$. The high-sound-intensity region at 5 km corresponds to the second side lobe with a grazing angle of $\pm 38^\circ$. The high-sound-intensity region at 2.2 km corresponds to the third side lobe with a grazing angle of $\pm 61^\circ$. Notably, the cutoff distance of the deep-sea bottom direct sound zone in the summer hydrological environment is about 18–19 km, and the sound field excited by directional sources does not significantly change the cutoff distance of the deep-sea bottom direct sound zone.

The distribution of sound fields excited by directional and omnidirectional sources during winter (with the presence of a 50 m surface waveguide) is shown in Fig. 5. In contrast with the excited sound field of an omnidirectional source, the main energy emitted by a directional source leads to a significant high-sound-intensity region at 18–23 km, which corresponds to the main lobe with a grazing angle of 0° in the directivity pattern. The leakage of the same side-lobe energy leads to intermittent high-sound-intensity regions within the range of 0–15 km. The high-sound-intensity region at 10 km corresponds to the first side lobe with a grazing angle of $\pm 21^\circ$. The high-sound-intensity region at 5 km corresponds to the second side



b) Freq = 1000 Hz, Sd = 10 m



c) Freq = 1000 Hz, Sd = 10 m

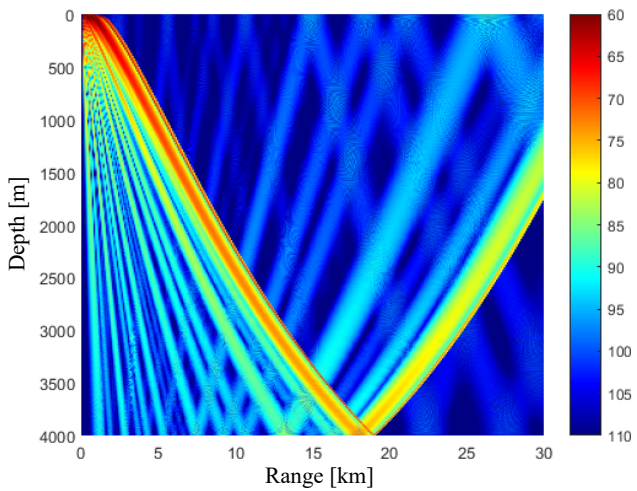
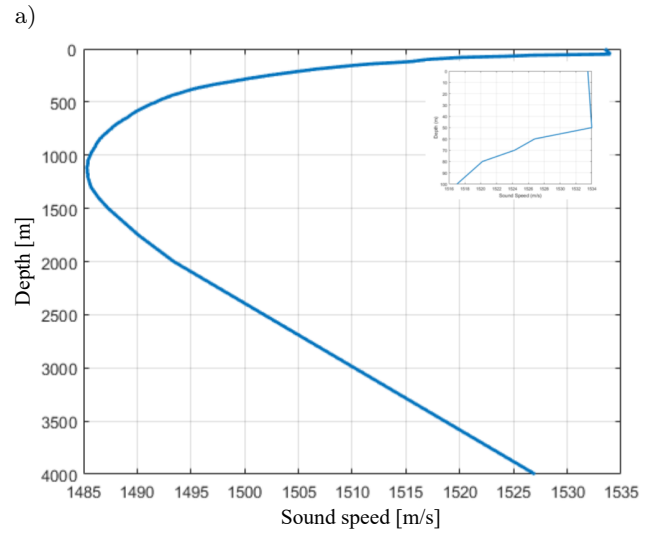
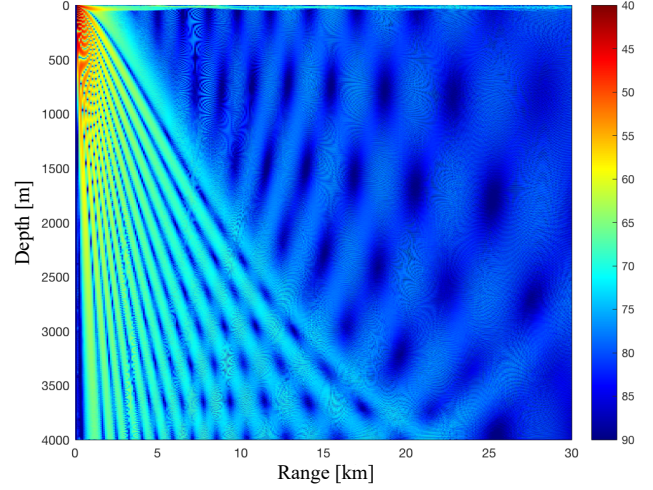


Fig. 4. Transmission loss during summer in the South China Sea: a) sound speed profile in summer; b) omnidirectional sources; c) directional sources.



b) Freq = 1000 Hz, Sd = 10 m



c) Freq = 1000 Hz, Sd = 10 m

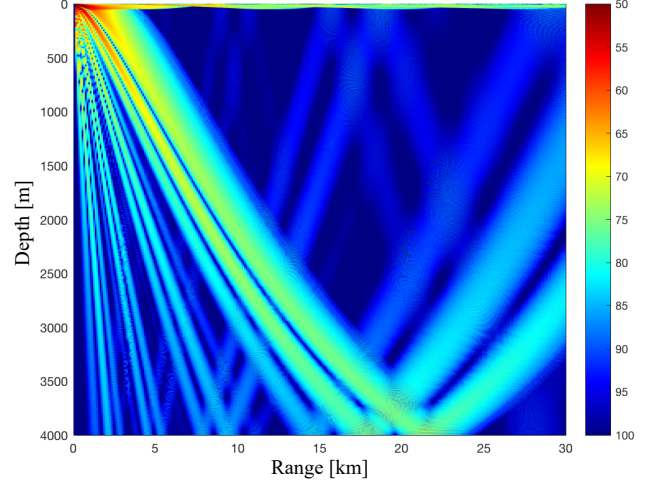


Fig. 5. Transmission loss during winter in the South China Sea: a) sound speed profile in winter; b) omnidirectional sources; c) directional sources.

lobe with a grazing angle of $\pm 38^\circ$. The high-sound-intensity region at 2.2 km corresponds to the third side lobe with a grazing angle of $\pm 61^\circ$. Notably, under the condition of omnidirectional source radiation, the cutoff distance of the deep-sea bottom that directly reaches the sound zone is about 22 km in the winter hydrological environment, which is far from the 18 km in the summer hydrological environment, because the surface waveguide leaks energy, causing it to propagate further. The cutoff distance of the sound field excited by the directional source from the seabed to the sound zone extends to 23–24 km, because the emission array beam-controlled emission within the surface waveguide layer causes more energy to concentrate on the surface waveguide layer. Moreover, the amount of energy leaked from the surface waveguide layer to the seabed to the direct sound zone increases.

On the basis of the analysis of the sound field characteristics in the direct sound zone of the deep-sea bottom under beam-controlled conditions, the next section analyzes the bottom reverberation characteristics in typical deep-sea environments.

4. Analysis of bottom reverberation intensity under beam-controlled emission conditions

Before analyzing and calculating deep-sea bottom reverberation intensity, obtaining the backscatter intensity of the seabed is necessary. For the simulation environment in Sec. 3, the seabed material is fine sand, and detailed parameters can be found in Sec. 3. On the basis of SSA to calculate backscatter intensity, the input rough spectral intensity of the model is 0.0004, and the rough spectral exponent is 2.6. On the basis of the aforementioned model parameters, the variation of the backscattering intensity of the deep-sea seabed with grazing angle is calculated at a frequency of 1 kHz. As shown in Fig. 6, the backscattering intensity of the rough interface increases with an increase

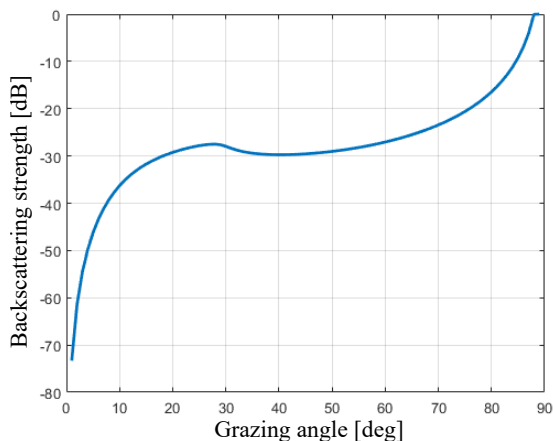


Fig. 6. Variation of seabed backscatter intensity with grazing angle.

in the grazing angle. This rough interface backscattering intensity is the input of the model for calculating bottom reverberation intensity.

On the basis of this scattering model and Eq. (3), combined with the sound field transfer function predicted by the ray model, the deep-sea bottom reverberation intensity excited by omnidirectional and directional sources under summer and winter conditions in the South China Sea is calculated.

The variation in deep-sea bottom reverberation intensity over time caused by omnidirectional and directional sources in the South China Sea during summer is shown in Fig. 7. For omnidirectional and directional sources, bottom reverberation occurs after 5 s, which corresponds to the time when bottom vertical reflected reverberation occurs. The reverberation intensity excited by omnidirectional sources monotonically decreases within 5 to 27 s, while the reverberation intensity excited by directional sources exhibits significant fluctuations within 5 to 27 s. This phenomenon exerts a significant effect on the active sonar target detection, resulting in intermittent reverberation masking and detectable areas.

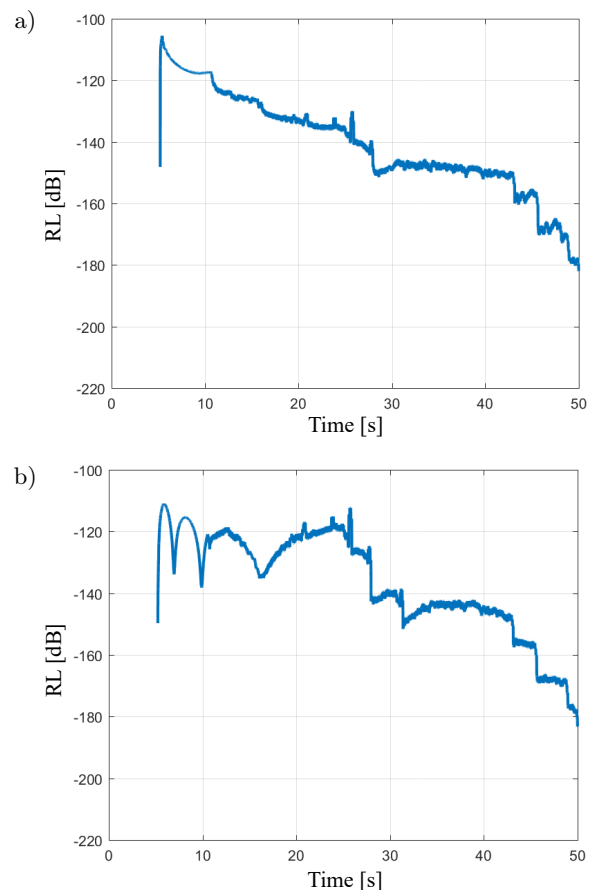


Fig. 7. Variation of bottom reverberation intensity with time: a) omnidirectional source; b) directional source.

By converting horizontal axis time into the acoustic path that corresponds to the active sonar, the variation

of deep sea bottom reverberation intensity excited by omnidirectional and directional sources in the South China Sea during summer with an acoustic path can be obtained, as shown in Fig. 8. Evident peaks are observed in the reverberation intensity at 4, 6, 9, and 18 km. This finding is related to the emission directionality of the eight-element vertical emission array.

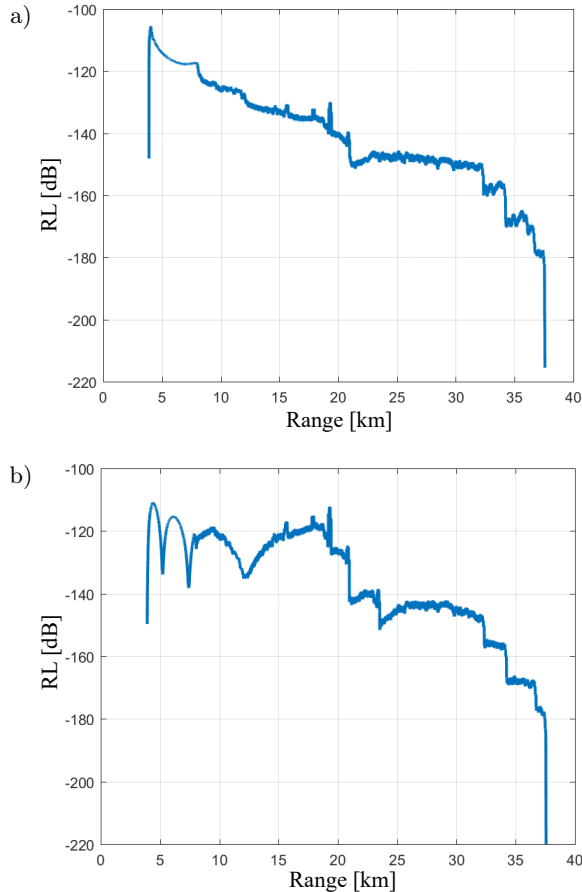


Fig. 8. Variation of bottom reverberation intensity with acoustic path: a) omnidirectional source; b) directional source.

To further illustrate the corresponding relationship among the peak values of intermittent bottom reverberation intensity, the bottom scattering area, and emission directionality, the acoustic path is converted into the horizontal distance from the transceiver array. The variation in deep-sea bottom reverberation intensity excited by omnidirectional and directional sources in the South China Sea during summer with a horizontal distance can be obtained as shown in Fig. 9. At a depth of 3995 m, the variation in propagation loss with horizontal distance is also given, as shown in Fig. 10. Comparing the variation of reverberation intensity in Fig. 9 with the variation of propagation loss in Fig. 10, four high-energy regions of reverberation intensity are observed, corresponding to the four high-energy regions of transmission loss and correspond-

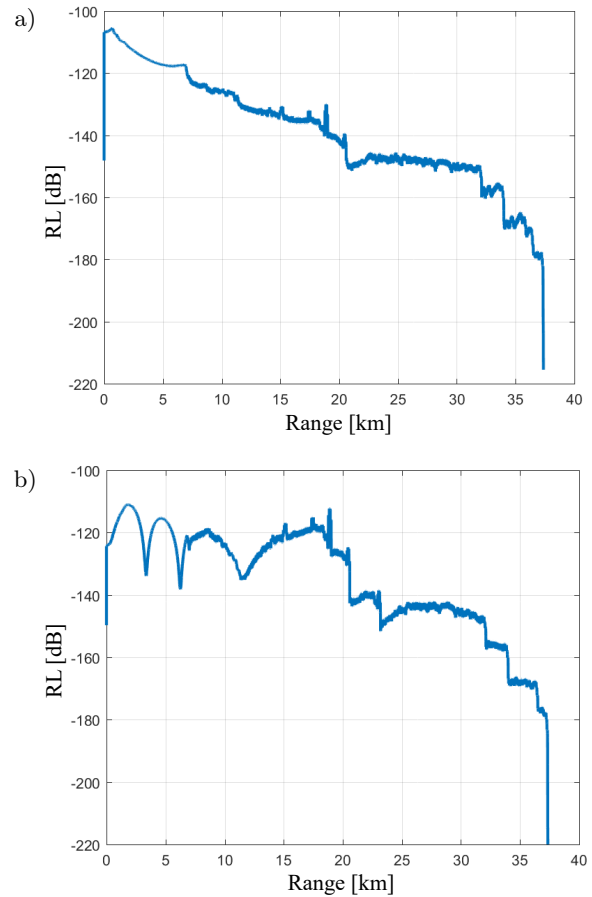


Fig. 9. Variation of bottom reverberation intensity with horizontal range: a) omnidirectional source; b) directional source.

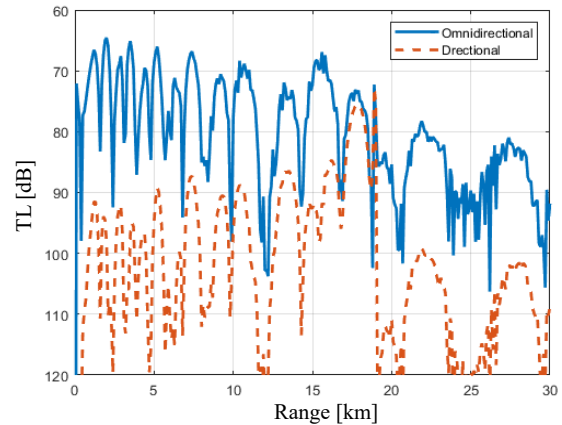


Fig. 10. Variation of transmission loss with horizontal range for a receiver depth of 3995 m. The blue solid line represents the transmission loss of sound field excited by an omnidirectional point source, while the red dashed line represents the transmission loss of sound field excited by a directional transmitter array.

ing to the main lobe and the three side lobes of directional sound sources. The high-reverberation zone that appears at 15–19 km corresponds to the main lobe with a grazing angle of 0° in the directivity pat-

tern. The leakage of side-lobe energy leads to intermittent high-reverberation zones within the range of 0–15 km. The high-reverberation zone at 10 km corresponds to the first side lobe with a grazing angle of $\pm 21^\circ$. The high-reverberation zone at 5 km corresponds to the second side lobe with a grazing angle of $\pm 38^\circ$. The high-reverberation zone at 2.2 km corresponds to the third side lobe with a grazing angle of $\pm 61^\circ$.

The variation of deep-sea bottom reverberation intensity over time caused by omnidirectional and directional sources in the South China Sea during winter is shown in Fig. 11. Similar to that during summer, bottom reverberation occurs after 5 s, which corresponds to the time when vertically reflected reverberation occurs on the seabed. The reverberation intensity excited by omnidirectional sources monotonically decreases within 5 to 30 s, while the reverberation intensity excited by directional sources exhibits significant fluctuations within 5 to 30 s. This phenomenon exerts a significant effect on the active sonar target detection, resulting in intermittent reverberation masking and detectable areas.

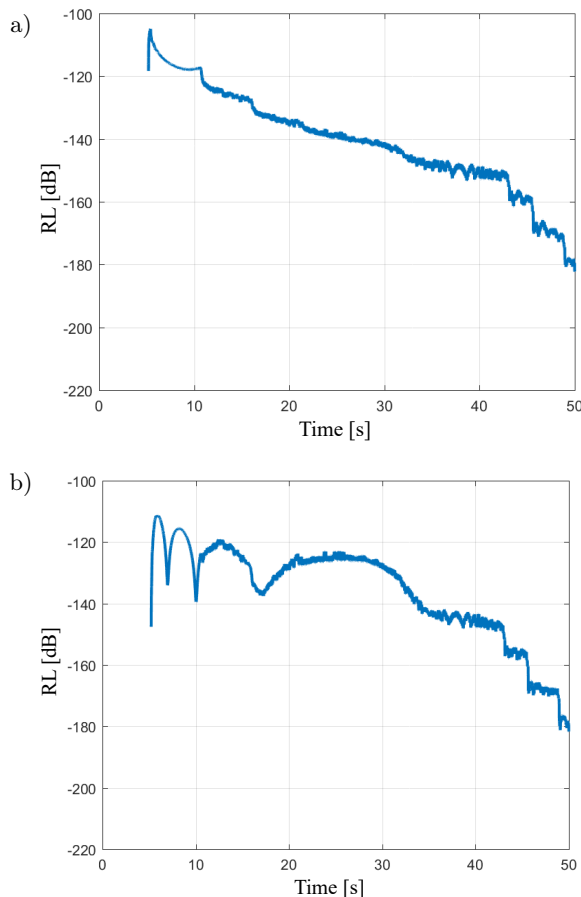


Fig. 11. Variation of bottom reverberation intensity with time: a) omnidirectional source; b) directional source.

By converting horizontal axis time into the acoustic path that corresponds to the active sonar, the variation of the deep-sea bottom reverberation intensity

excited by omnidirectional and directional sources in the South China Sea during winter can be obtained with respect to the acoustic path, as shown in Fig. 12. Evident peaks can be seen in the reverberation intensity at 4, 6, 9, and 20 km. These peaks are related to the emission directionality of the eight-element vertical emission array.

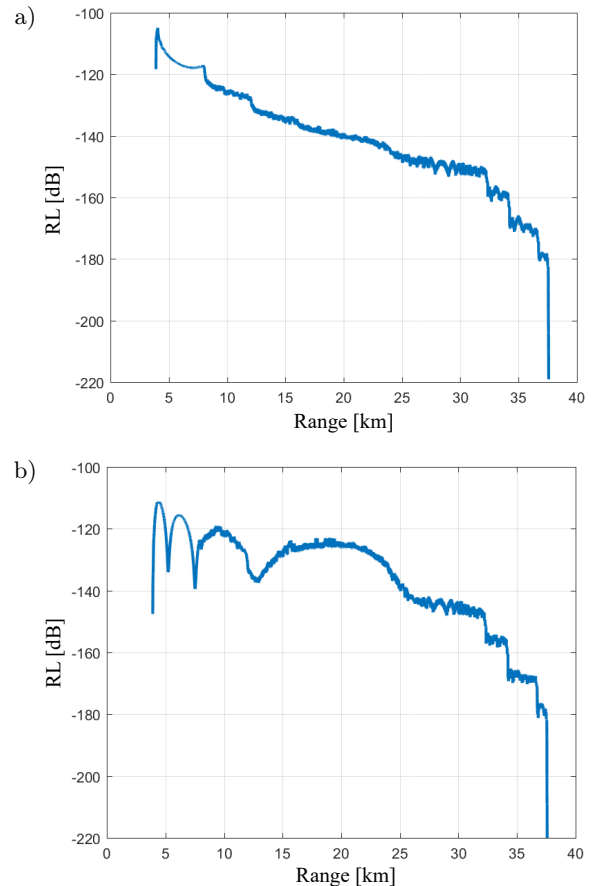


Fig. 12. Variation of bottom reverberation intensity with acoustic path: a) omnidirectional source; b) directional source.

To further illustrate the corresponding relationship among the peak value of intermittent bottom reverberation intensity, bottom scattering area, and emission directionality, the acoustic path is converted into the horizontal distance from the transceiver array. The variation of deep-sea bottom reverberation intensity excited by omnidirectional and directional sources in the South China Sea during winter with horizontal distance can be obtained as shown in Fig. 13. At a depth of 3995 m, the variation in transmission loss with the horizontal distance is also given, as shown in Fig. 14. Comparing the variation of reverberation intensity in Fig. 13 with the variation of transmission loss in Fig. 14, four high-energy regions of reverberation intensity can also be observed, corresponding to the four high-energy regions of transmission loss and corresponding to the main lobe and three side lobes

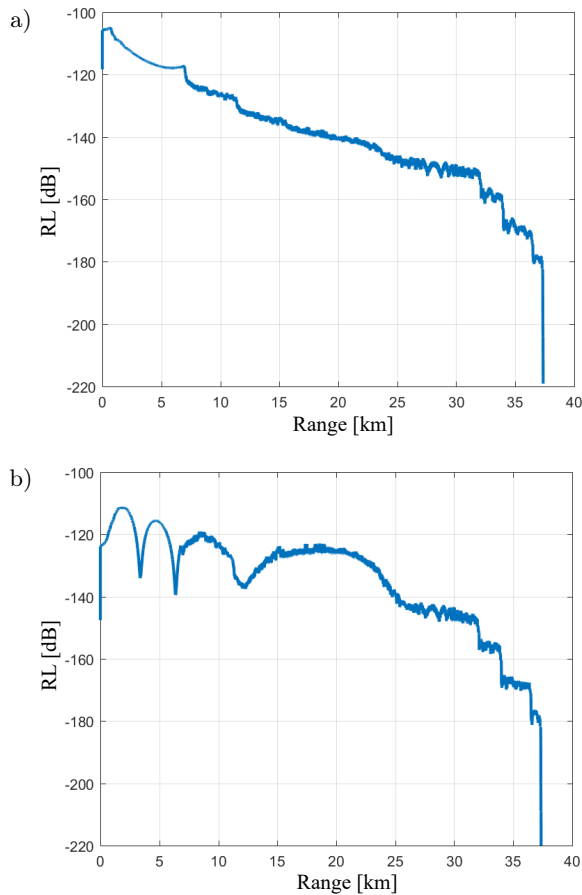


Fig. 13. Variation of bottom reverberation intensity with horizontal range: a) omnidirectional source; b) directional source.

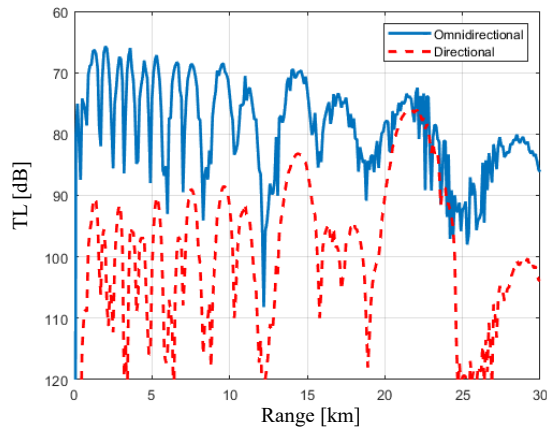


Fig. 14. Variation of transmission loss with horizontal range for a receiver depth of 3995 m. The blue solid line represents the transmission loss of sound field excited by an omnidirectional point source, while the red dashed line represents the transmission loss of sound field excited by a directional transmitter array.

of directional sound sources. The high reverberation zone appearing at 15–23 km corresponds to the main lobe with a grazing angle of 0° in the directivity pat-

tern. The leakage of side-lobe energy leads to intermittent high-reverberation zones within the range of 0–15 km. The high-reverberation zone at 10 km corresponds to the first side lobe with a grazing angle of $\pm 21^\circ$. The high-reverberation zone at 5 km corresponds to the second side lobe with a grazing angle of $\pm 38^\circ$. The high-reverberation zone at 2.2 km corresponds to the third side lobe with a grazing angle of $\pm 61^\circ$.

To compare the differences in the distribution of bottom reverberation intensity caused by beam-controlled emission in the South China Sea during summer and winter, Figs. 10 and 14 were drawn together, as shown in Fig. 15. Except for the differences in hydrological conditions (sound speed profile), the two curves are plotted under the same simulation conditions. The variation trend of reverberation intensity within a range of 12 km is nearly consistent, including the high-reverberation zone caused by side-lobe energy leakage. However, significant differences exist in the high-reverberation zone caused by the directional main lobe emission. The major issues are:

- 1) For the high-reverberation zone near a range of 18 km excited by the main lobe energy, bottom reverberation intensity during winter is weaker than that during summer, because the existence of an isothermal layer on the surface during winter results in most of the energy radiated by small grazing angles being bound to the surface waveguide layer. The energy reaching the direct sound zone on the seabed beyond 15 km is lower than that in the absence of a surface waveguide layer.
- 2) For the high-reverberation zone excited by the main lobe energy, the duration (corresponding horizontal distance) of the main lobe's high-reverberation zone is longer during winter, and the effect on the active target detection in deep-sea environments is more significant. The reason for this finding is that after the beam-controlled

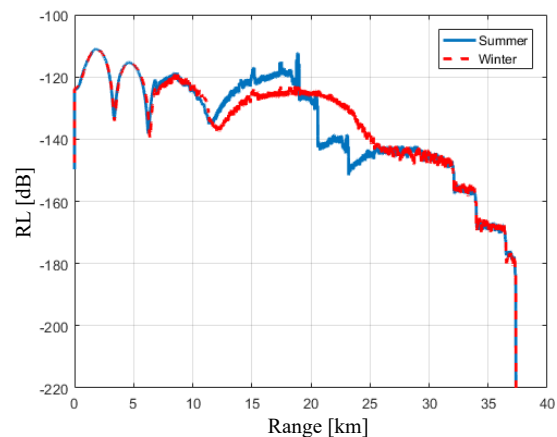


Fig. 15. Bottom reverberation during summer and winter under beam-controlled emission conditions.

emission of the emission array inside the surface waveguide layer, the sound energy leakage of the surface waveguide layer expands the direct sound zone of the deep sea during winter, and the acoustic ray with a small grazing angle can reach up to 23 km, resulting in an increase in the duration of the main lobe's high-reverberation zone.

5. Conclusions

In response to the challenge of analyzing the intensity of bottom reverberation in typical deep-sea environments, this study proposes a prediction method for the intensity of bottom reverberation under beam-controlled (shaded) emission conditions and explains the variation law of bottom reverberation intensity under beam-controlled emission conditions through theoretical and simulation analyses in typical deep-sea environments of the South China Sea with a seabed material of fine sand. The conclusions drawn are:

- 1) Deep-sea bottom reverberation intensity under beam-controlled emission conditions exhibits significant fluctuations during the duration of reverberation in the direct sound zone of the seabed. This phenomenon is closely related to the directionality of source emission, leading to intermittent reverberation masking and detectable areas in the active sonar detection.
- 2) For the high-reverberation zone near the cutoff distance of the direct sound from the seabed excited by the main lobe energy of the directional source, the reverberation intensity during winter is weaker than that during summer. The reason for this finding is that the existence of a surface isothermal layer during winter results in most of the energy emitted by the small grazing angle being bound to the surface waveguide layer. Meanwhile, the energy reaching the cutoff distance of the direct sound from the seabed is lower than that without surface waveguide layer.
- 3) Under the beam-controlled emission conditions of the emission array located within the surface waveguide layer of the deep sea during winter, the duration of the high-reverberation zone near the cutoff distance of the direct sound from the seabed is longer, because the sound energy leakage from the surface waveguide layer expands the direct sound zone of the deep sea during winter. The acoustic ray with a small grazing angle can reach further distance, resulting in an increase in the duration of the high-reverberation zone of the main lobe. This phenomenon will have a more significant effect on the active target detection in deep-sea environments.

The analysis of the distribution characteristics of deep-sea bottom reverberation intensity in this study

provides guidance for the suppression of deep-sea active sonar reverberation, and the evaluation and reasonable application of deep-sea active sonar detection performance in actual combat.

Acknowledgments

This research was funded by National Natural Science Foundation of China (grant no. 12304501), Science and Technology on Sonar Laboratory foundation (grant no. 2022-JCJQ-LB-031-02), and Youth Elite Scientists Sponsorship Program by CAST (grant no. YESS20200330).

References

1. BROSCHE S.L., THORSOS E.I. (1997), An investigation of the small slope approximation for scattering from rough surfaces. Part II. Numerical studies, *The Journal of the Acoustical Society of America*, **101**(5): 2615–2625, doi: [10.1121/1.418502](https://doi.org/10.1121/1.418502).
2. COLLINS M.D., EVANS R.B. (1992), A two-way parabolic equation for acoustic backscattering in the ocean, *The Journal of the Acoustical Society of America*, **91**(3): 1357–1368, doi: [10.1121/1.402465](https://doi.org/10.1121/1.402465).
3. CUI X., CHI C., LI S., LI Z., LI Y., HUANG H. (2023), Waveform design using coprime frequency-modulated pulse trains for reverberation suppression of active sonar, *Journal of Marine Science and Engineering*, **11**(1): 28, doi: [10.3390/jmse11010028](https://doi.org/10.3390/jmse11010028).
4. ELLIS D.D., CROWE D.V. (1991), Bistatic reverberation calculations using a three-dimensional scattering function, *The Journal of the Acoustical Society of America*, **89**(5): 2207–2214, doi: [10.1121/1.400913](https://doi.org/10.1121/1.400913).
5. ELLIS D.D., HALLER D.R. (1987), A scattering function for bistatic reverberation calculations, *The Journal of the Acoustical Society of America*, **82**(1): 124, doi: [10.1121/1.2024654](https://doi.org/10.1121/1.2024654).
6. GRAUSS R.C., GRAGG R.F., WURMSER D., FIALKOWSKI J.M., NERO R.W. (2002), *Broadband models for predicting bistatic bottom, surface and volume scattering strengths*, Naval Research Laboratory Report.
7. GUO X.Y., SU S.J., WANG Y.K. (2009), Research on the signal modeling method for sea bottom reverberation based on ray theory [in Chinese], *Technical Acoustics*, **28**(3): 203–207.
8. HAO Y. *et al.* (2023), Underwater reverberation suppression via attention and cepstrum analysis-guided network, *Journal of Marine Science and Engineering*, **11**(2): 313, doi: [10.3390/jmse11020313](https://doi.org/10.3390/jmse11020313).
9. LUPIEN V.H., BONDARYK J.E., BAGGEROER A.B. (1995), Acoustical ray-tracinginsonification software modeling of reverberation at selected sites near the

- Mid-Atlantic Ridge, *The Journal of the Acoustical Society of America*, **98**(5): 2987, doi: [10.1121/1.413929](https://doi.org/10.1121/1.413929).
10. MACKENZIE K.V. (1961), Bottom reverberation for 530- and 1030-cps sound in deep water, *The Journal of the Acoustical Society of America*, **33**(11): 1498–1504, doi: [10.1121/1.1908482](https://doi.org/10.1121/1.1908482).
 11. PORTER M.B. (2011), *The Bellhop Manual and User's Guide: Preliminary Draft*.
 12. QIN J.X., WANG L.H., LI Z.L. (2019), Theory and experiment of large-depth reverberation in deep water [in Chinese], *Technical Acoustics*, **38**(5): 95–96.
 13. THORSOS E.I., BROSCHE S.L. (1995), An investigation of the small slope approximation for scattering from rough surfaces. Part I. Theory, *The Journal of the Acoustical Society of America*, **97**(4): 2082–2093, doi: [10.1121/1.412001](https://doi.org/10.1121/1.412001).
 14. URICK R.J., SALING D.S. (1962), Backscattering of explosive sound from the deep-sea bed, *The Journal of the Acoustical Society of America*, **34**(11): 1721, doi: [10.1121/1.1909106](https://doi.org/10.1121/1.1909106).
 15. WENG J.B., LI F.H., LIU J.J. (2014), The preliminary study on bottom reverberation model in deep water [in Chinese], *Technical Acoustics*, **33**(S2): 71–73.
 16. WILLIAMS K.L., JACKSON D.R. (1998), Bistatic bottom scattering: Model, experiments, and model data comparison, *The Journal of the Acoustical Society of America*, **103**(1): 169–181, doi: [10.1121/1.421109](https://doi.org/10.1121/1.421109).
 17. XU L., YANG K., GUO X., LI H. (2016), Bistatic bottom reverberation in deep ocean: Modeling and data comparison, [in:] *OCEANS 2016 – Shanghai*, pp. 1–5, doi: [10.1109/OCEANSAP.2016.7485385](https://doi.org/10.1109/OCEANSAP.2016.7485385).
 18. XUE R.Z., DUAN R., YANG K.D., MA Y.L., GUO Y. (2021), Modeling and analysis of monostatic incoherent boundary reverberation intensity in deep water, *Acta Acoustica*, **46**(6): 926–938, doi: [10.15949/j.cnki.0371-0025.2021.06.014](https://doi.org/10.15949/j.cnki.0371-0025.2021.06.014).
 19. ZHANG R.H., JIN G.L. (1987), Normal-mode theory of the average reverberation intensity in shallow water, *Journal of Sound and Vibration*, **119**(2): 215–223, doi: [10.1016/0022-460X\(87\)90450-0](https://doi.org/10.1016/0022-460X(87)90450-0).